

Vacuum preloading and PVDs in soft soils beneath embankments: 3D coupled analysis incorporating overall stability study

José Leitão Borges^{1#} 

Article

Keywords

Prefabricated vertical drains
Vacuum preloading
Soft soil
Three-dimensional modelling
Overall stability
Mechanical-hydraulic coupled analysis

Abstract

Although embankments on soft soils with prefabricated vertical drains (PVDs) under vacuum preloading have been widely studied, there is a lack of studies in the literature in which overall stability is analysed through three-dimensional (3D) mechanical-hydraulic coupled modelling. In order to contribute to overcome such deficiency, this paper presents 3D numerical analyses of an embankment on soft soils incorporating PVDs and vacuum preloading. A finite element code, which includes 3D fully coupled analysis, is used and a method for overall stability study – which uses the 3D numerical results obtained with the finite element code – is presented and applied. A parametric study is performed in order to analyse the influence of the magnitude of the vacuum preload and the staged construction of the embankment (time of vacuum application before completion of the embankment). Overall stability, excess pore pressures, settlements, horizontal displacements and stress levels are analysed.

1. Introduction

Due to the geotechnical characteristics of the soft soils, such as low strength, high compressibility and low permeability, a number of techniques are available in practice to improve the behaviour of embankments built on such soils. Such improvement techniques provide one or more of the following effects: increase of overall stability, consolidation acceleration and reduction of long-term settlements.

The two techniques most used in practice when the main purpose is to accelerate the consolidation are: (i) use of prefabricated vertical drains (PVDs) (Holtz et al., 1991; Hird et al., 1992; Chai et al., 1995; Borges, 2004; Shen et al., 2005; Lin & Chang, 2009; Liu & Rowe, 2015; Zhang et al., 2015); (ii) preloading, which can typically be performed by an embankment surcharge or vacuum suction (Zhang et al., 2018; Lam et al., 2015; Bergado et al., 2002; Cascone & Biondi, 2013; Long et al., 2015; Indraratna et al., 2016; Mesri & Khan, 2012; Rujikiatkamjorn et al., 2008).

Surcharge preloading combined with PVDs is a popular technique to further increase the consolidation acceleration or reduction of the construction time (Lam et al., 2015). Typically, the PVDs are installed into the soft ground, followed by the construction of the embankment and the surcharge

application. However, this technique is often limited in terms of the magnitude of the surcharge that can be applied, due to overall instability of the embankment. In that case, the use of PVDs combined with vacuum preloading is an alternative that solves the problems of the conventional surcharge preloading (Saowapakpiboon et al., 2010; Rujikiatkamjorn et al., 2008; Long et al., 2015; Chai et al., 2005; Chai & Rondonuwu, 2015; Saowapakpiboon et al., 2010; Indraratna et al., 2012). The advantage of the vacuum application is that gradients of pore pressure are induced in the ground – provoking therefore the consolidation process (pore pressure reduction and effective mean stress increase) – maintaining a constant total stress, instead of what happens in conventional surcharge preloading. Besides a better performance in terms of stability, the vacuum technique also provides lower outward and upward displacements in the lateral regions of the embankment.

Although PVDs combined with vacuum preloading have been widely studied, there is a lack of studies in the literature in which overall stability is analysed through three-dimensional mechanical-hydraulic coupled modelling. In this paper, in order to contribute to overcome such deficiency, three-dimensional numerical analyses are performed and a method for overall stability study – which uses the 3D results of a finite element code – is proposed and applied.

#Corresponding author. E-mail address: leitao@fe.up.pt

¹Universidade do Porto, Construct, Faculdade de Engenharia, Porto, Portugal.

Submitted on July 25, 2021; Final Acceptance on April 21, 2022; Discussion open until November 30, 2022.

<https://doi.org/10.28927/SR.2022.072821>



This is an Open Access article distributed under the terms of the Creative Commons Attribution License, which permits unrestricted use, distribution, and reproduction in any medium, provided the original work is properly cited.

A parametric study is performed so that the influence of the following parameters is studied: magnitude of the vacuum preload; staged construction of the embankment (time of vacuum application before completion of the embankment). Overall stability, excess pore pressures, settlements, horizontal displacements and stress levels are analysed.

2. Finite element code

The finite element code used herein was developed by Borges (1995). The initial version (2-D version) was presented in 1995 and several improvements were subsequently developed and implemented, particularly a 3D version (Borges, 2004). Among other features, the code incorporates fully mechanical-hydraulic coupled analysis (Biot consolidation theory) (Borges, 1995; Lewis & Schrefler, 1987; Britto & Gunn, 1987) and the p - q - θ critical state model for soil constitutive simulation (Borges, 1995; Lewis & Schrefler, 1987).

The p - q - θ model is an extension of the Modified Cam-Clay model into the three-dimensional stress space that uses the Mohr-Coulomb surface as the critical state criterion, while in the Modified Cam-Clay model the Drucker-Prager surface is utilised. Therefore, in the p - q - θ model, the parameter that defines the slope of the critical state line, M , is not constant (as happens in the Modified Cam-Clay model) and depends on the angular stress invariant θ and effective friction angle, ϕ' , as follows (Lewis & Schrefler, 1987; Borges, 1995):

$$M = \frac{3\sin\phi'}{\sqrt{3}\cos\theta + \sin\phi'\sin\theta} \tag{1}$$

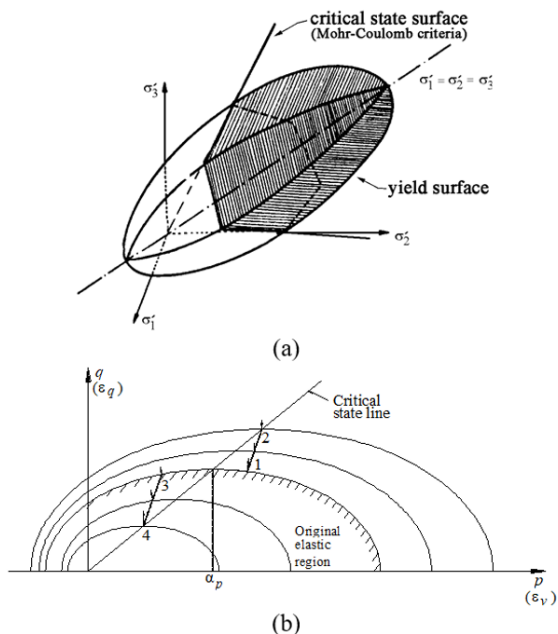


Figure 1. Yield and critical state surfaces of the p - q - θ critical state model in (a) principal effective stress space and (b) p - q space.

The Mohr-Coulomb criterion is defined when M , given by Equation 1, is introduced in the equation of the critical state line

$$q = M \cdot p \tag{2}$$

where p is the effective mean stress and q the deviatoric stress.

The yield and critical state surfaces of the p - q - θ model in the principal effective stress space and in the p - q plane are shown in Figure 1. Depending on the over-consolidation ratio, hardening behaviour or softening behaviour is modelled. Hardening occurs in normally consolidated or lightly over-consolidated clays (stress path 1-2, in Figure 1b) while softening occurs in moderately to strongly over-consolidated clays (stress path 3-4, in Figure 1b).

The finite element code has been used to analyse a wide range of geotechnical structures involving consolidation (Borges, 1995; Borges & Cardoso, 2001, 2002; Costa, 2005; Domingues, 2006; Costa et al., 2007; Marques, 2008; Borges et al., 2009; Guerra, 2009; Azevedo, 2010; Borges & Marques, 2011; Caramelo, 2011; Monteiro, 2011; Pinto, 2011; Alves, 2012; Gonçalves, 2012; Borges & Guerra, 2014; Santos, 2014; Barros, 2015; Borges & Gonçalves, 2016; Borges & Almeida, 2018; Marques, 2021).

Comparing numerical and field results, good agreements were obtained in the modelling of several case studies, such as: (i) two trial geosynthetic-reinforced embankments on soft soils (Borges, 1995), one constructed up to failure and the other, also incorporating prefabricated vertical drains, observed until the end of consolidation; (ii) two embankments on soft soils reinforced with stone columns, one in the Gold Coast Highway of Australia (Marques, 2021), and the other in the northern railway of Portugal (Domingues, 2006); (iii) a braced excavation in very soft ground carried out in the City of San Francisco (Costa et al. 2007; Costa, 2005).

For 3D analysis, two types of the 20-noded brick element are used: (i) the coupled element (Figure 2a), for

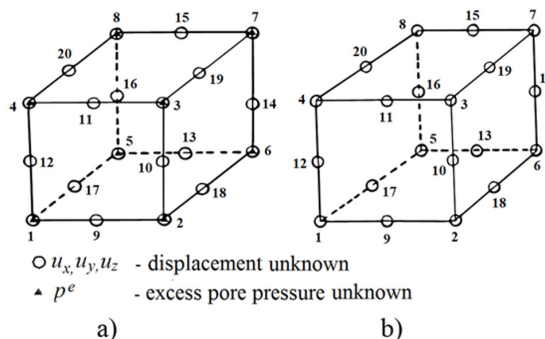


Figure 2. 20-noded brick element: (a) coupled element, with 60 displacement degrees of freedom and 8 excess pore pressure degrees of freedom; (b) non-coupled element, with 60 displacement degrees of freedom.

the soft soil, where consolidation is considered; (ii) the non-coupled element (Figure 2b), for the embankment material. All the twenty nodes of the coupled element have displacement degrees of freedom while only the 8 vertex nodes have excess pore pressure degrees of freedom. The 20 nodes of a non-coupled element have only displacement degrees of freedom.

3. Overall stability analysis

3.1 Preamble

Especially due to their simplicity, limit equilibrium methods have been commonly used in practice to evaluate overall stability of embankments on soft soils. Theoretically, however, because rigid-plastic behaviour is tacitly assumed for the materials (soils and other materials – geosynthetics or soil-cement, for instance, if reinforcement is used), the use of such methods may raise some limitations, since strains before overall failure, as well as stress redistribution due to elastoplastic behaviour of the materials, are not taken into account in the analysis.

An alternative approach that overcomes such limitations is the use of finite element (FE) modelling (Rowe & Soderman, 1987; Borges, 1995; Borges & Cardoso, 2002; Hinchberger & Rowe, 2003; Chen et al., 2015; Da Silva et al., 2017). In the context of embankments on soft soils, the finite element modelling in stability studies has been mostly based on two-dimensional analysis. However, in many cases, the embankment behaviour is clearly three-dimensional, like, for instance, when PVDs, stone or soil-cement columns are installed into the soft ground. Although in a macro-level one may say that an embankment on soft soils incorporating PVDs is approximately a plane strain problem (if its longitudinal length is large), in fact it is clearly a 3D problem – both mechanical and hydraulic – in a slice of the domain between two vertical planes normal to the longitudinal direction, one containing one row of drain centres and the other equidistant from two rows of drains (Borges & Almeida, 2018). Under these conditions, the 3D finite element analysis only needs to simulate such slice of the domain, where, due to symmetry conditions, zero-displacement conditions in the longitudinal direction are set on the boundary planes normal to the longitudinal direction. Also due to symmetry conditions, water flow crossing such planes, modelled as impermeable boundaries, is not allowed.

A method for 3D overall stability analysis, which uses the results of the finite element code, is presented and applied in this paper. This method is an extension for 3D analysis from the 2D method presented by Borges & Cardoso (2002) and can be applied when the 3D domain of the finite element analysis is a slice between two vertical planes normal to the longitudinal direction of the problem (like for PVDs beneath embankments, as mentioned).

3.2 Proposed method for 3D overall stability analysis

For any stage of a 3D problem whose FE domain is a slice between two vertical planes normal to the longitudinal direction (z -axis in Figure 3), using the finite element results, the stability analysis program computes the overall safety factor, F , by analysing the stability along a large number of potential slip cylindrical surfaces whose axes are parallel to z -axis and cross-sections are circular (Figure 3). The slip surfaces are chosen with criterion; their cross-sections are defined considering a mesh of circle centres and, for each centre, several concentric circles with the radius varying from a minimum to a maximum value. The smallest value of safety factor obtained defines the critical slip surface and quantifies the problem safety.

For a particular potential failure surface, the proposed method firstly determines the intersection points of the cylindrical surface with the edges of the finite elements of the 3D-mesh. Therefore, the potential failure surface is divided into small polygons (typically, a quadrilateral; Figure 4), each of them located inside of only one of the finite elements of the mesh.

Thereafter, the average values of σ'_x , σ'_y , σ'_z and τ_{xy} , τ_{yz} , τ_{zx} normal and shear stresses in the xyz -space (where z is the longitudinal direction), at each of those polygons, are computed extrapolating from stresses at the Gauss points of the corresponding finite element.

Considering the slip surface divided into polygons, the safety factor is computed as follows:

$$F = \frac{\sum_{i=1}^N \tau_i A_i}{\sum_{i=1}^N \tau_{fi} A_i} \quad (3)$$

where: τ_i – projection of the acting shear stress at the i -polygon on the slip direction (i.e. normal to z -axis), determined from

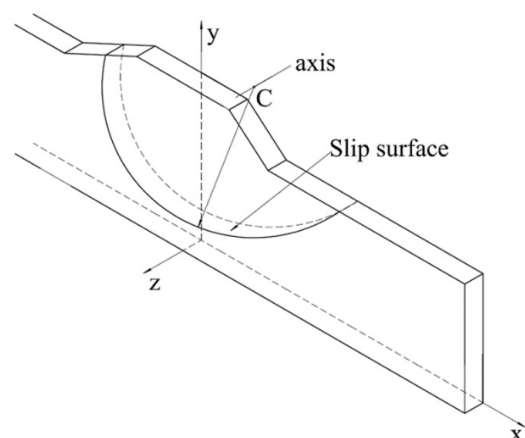


Figure 3. 3D scheme of a potential slip cylindrical surface.

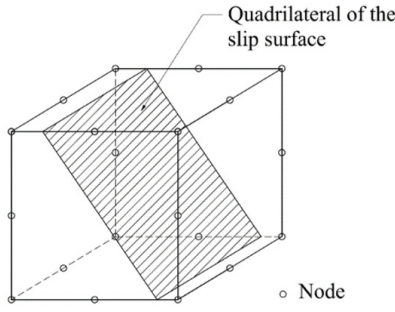


Figure 4. Quadrilateral of the slip surface within a 20-noded brick element.

effective stresses σ'_x , σ'_y and τ_{xy} , known the angle that the i -polygon plane makes with x -axis (it should be noted that τ_i , normal to z -axis, is not function of σ'_z , τ_{yz} and τ_{zx}); τ_{fi} – soil shear strength at i -polygon; A_i – i -polygon area; N – number of mesh elements intersected by the failure surface.

Taking into account that a critical state model is used in the finite element analysis, the soil shear strength τ_{fi} – which varies with the consolidation – is calculated by the following equation of the critical state soil mechanics (Britto & Gunn, 1987; Borges & Santos, 2020):

$$\tau_{fi} = \frac{1}{2} M \cdot \exp\left(\frac{\Gamma - v_i}{\lambda}\right) \quad (4)$$

where M is obtained by Equation 1 and v_i , the specific volume of soil at i -polygon, is calculated as follows:

$$v_i = \Gamma - k \ln p_i - (\lambda - k) \ln \alpha_{pi} \quad (5)$$

At the i -polygon, α_{pi} is the p -value of the centre of the yield surface in p - q plane (Figure 1b), extrapolated from α_p -values at Gauss points; $p_i = (\sigma'_{xi} + \sigma'_{yi} + \sigma'_{zi})/3$ is the effective mean stress; λ , k and Γ are parameters of the p - q - θ model (soil properties), defined as follows: λ , slope of normal consolidation line and critical state line; k , slope of swelling and recompression line; Γ , specific volume of soil on the critical state line at mean normal effective stress equal to 1 kPa.

When the problem is symmetric and the finite element mesh does not include the entire domain, if part of the slip surface is outside the FE mesh (Figure 5), a complementary symmetric surface is considered, so that the results of such part are obtained from the complementary surface.

4. Description of the problem

The problem comprises the construction of a 3.0 m-high symmetric embankment, with a 15 m-wide crest, 1 / 1.5 (V/H) inclined slopes and large longitudinal length (Figure 6). The

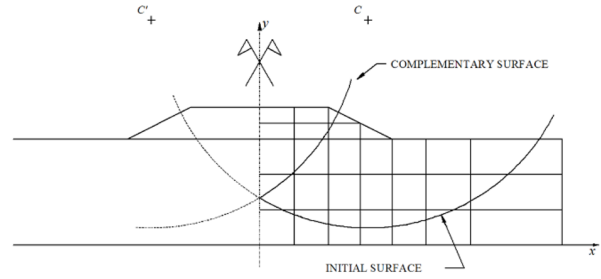


Figure 5. Slip surface of a symmetric problem that does not include the entire domain.

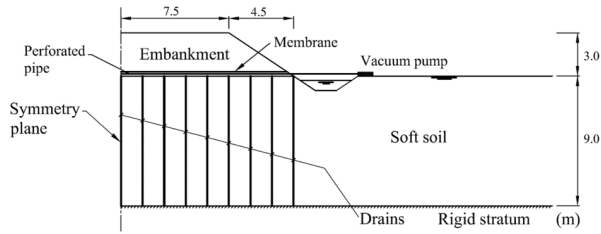


Figure 6. Vertical cross section of the problem.

soft ground is a 9 m-thick saturated clay lying on a rigid and impermeable stratum. The water level is at the ground surface. PVDs ($100 \times 5 \text{ mm}^2$) are installed at 1.5 m spacing in a square pattern and combined with vacuum preloading. Similarly to what was installed in a case study for a storage yard at Tianjin Port, China (Rujikiatkamjorn et al., 2008), a 0.30 m sand blanket is supposed to serve as a platform for placing horizontal perforated pipes required for applying and redistributing the vacuum pressure (Figure 6). Horizontal drainage (pipes wrapped in geotextile filters) covered with impermeable membranes is laid to connect the PVDs to the vacuum pump. Parameters related to the PVDs are shown in Table 1.

Regarding the time evolution of the embankment fill and the vacuum application, five cases (C1-C5) are considered (Figure 7), so that the overall stability of the embankment is analysed, as well as the influence of the magnitude of the vacuum pressure and time of vacuum application before completion of the embankment (staged construction). The duration of the embankment construction is 11 days for cases C1 and C2 and 50 days for cases C3, C4 and C5. Vacuum pressure is not applied in cases C1 and C5 (only PVDs are used). A vacuum pressure of -60 kPa is applied in cases C2 and C3 while -90 kPa is applied in case C4. The duration of vacuum application after the end of construction – 60 days for cases C2 and C3 and 30 days for case C4 – was set so that the embankment settlement after the end of vacuum application is negligible. For case C2 – which has the same constructive sequence as case C1 – this corresponds to withdraw the vacuum application at the instant in which its

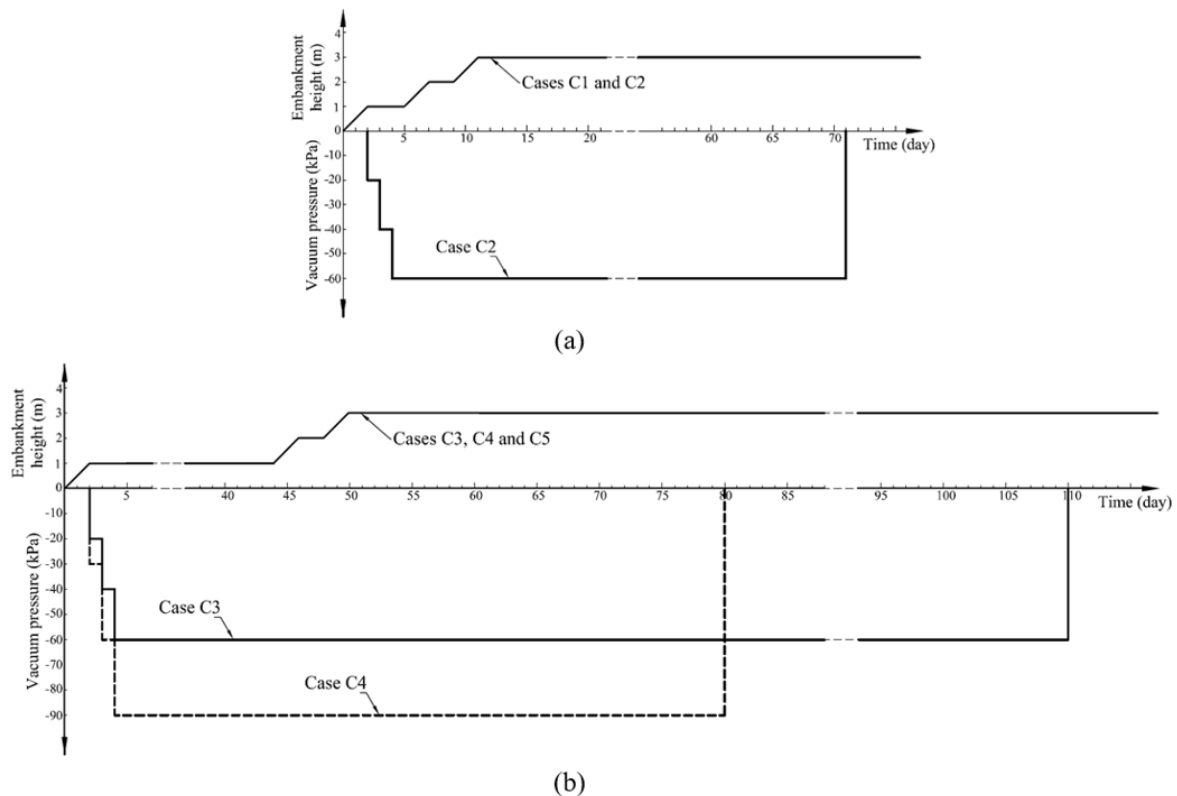


Figure 7. Staged construction and vacuum pressure: (a) cases C1 (without vacuum) and C2; (b) cases C3, C4 and C5 (without vacuum).

Table 1. Parameters related to the PVDs.

Spacing	1.5 m
Vertical length	9.0 m
Cross-section of PVD	100 × 5 mm ²
Discharge capacity, q_w	130 m ³ / year (per drain)
Cross-section of mandrel	120 × 60 mm ²
Cross-section of smear zone	240 × 120 mm ²

settlement is approximately equal to the long-term settlement of the case without vacuum application (case C1).

Considering the variation of only one parameter, the magnitude of the vacuum pressure is the unique parameter that varies from case C1 (vacuum pressure, $p_v = 0$) to case C2 ($p_v = -60$ kPa), as well as from case C5 ($p_v = 0$) to cases C3 ($p_v = -60$ kPa) and C4 ($p_v = -90$ kPa). Regarding the other parameter analysed, the time of vacuum application before completion of the embankment, its influence can be analysed comparing the results of cases C2 and C3.

Figure 8 shows the three-dimensional finite element mesh of the problem.

The displacement boundary conditions are defined taking into account that the soft clay lays on a rigid stratum ($y = 0$ plane, where displacements are set as zero in the three directions, x , y and z). On the other hand, symmetry conditions imply: (i) zero displacement in x -direction for nodes on the $x = 0$ plane; (ii) zero displacement in z -direction for nodes

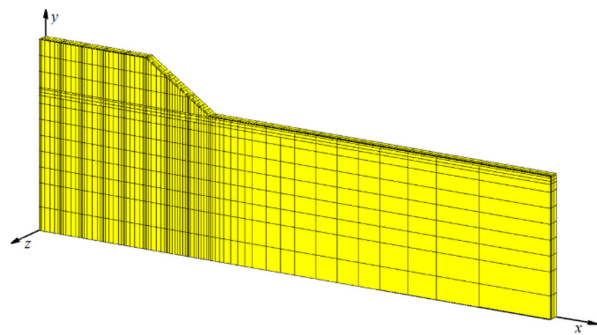


Figure 8. 3D finite element mesh of the problem.

on the $z = 0.75$ m plane, vertical plane containing one row of drain centres; (iii) zero displacement in z -direction for nodes on the $z = 0$ plane, vertical plane equidistant from two rows of drains in x -direction. Assuming that the horizontal displacement can be set as zero at nodes which are enough distant from the embankment, the plane of $x = 36$ m is considered as the lateral boundary with zero displacement in x -direction.

In hydraulic terms, to simulate the vacuum pressure, negative values for excess pore pressure are set on the drainage surfaces defined by the drains considered as sheets, namely on the following planes: $x = 0$, $x = 1.5$, $x = 3.0$, $x = 4.5$, $x = 6.0$, $x = 7.5$, $x = 9.0$, $x = 10.5$ and $x = 12$ m,

with y -coordinate ranging from 0 to 9 m and z -coordinate from 0.70 to 0.75 m (which means that centres of the drains are located on the $z = 0.75$ m boundary plane and each drain is installed with its larger dimension, 0.10 m, in z -direction). The vacuum pressure was assumed to be constant along the entire depths of PVDs, as observed in the case study described by Rujikiatkamjorn et al. (2008). The well resistance was neglected due to the very high discharge capacity of the drain, i.e., $q_w > 120$ m³/year (Indraratna & Redana, 2000).

The constitutive behaviour of soils (embankment material and clay) is simulated with the p - q - θ critical state model whose parameters are indicated in Table 2 (λ , slope of normal consolidation line and critical state line; k , slope of swelling and recompression line; Γ , specific volume of soil on the critical state line at mean normal effective stress equal to 1 kPa; N , specific volume of normally consolidated soil at mean normal effective stress equal to 1 kPa). Table 2 also shows other geotechnical properties: γ , unit weight; ν' , Poisson's ratio for drained loading; ϕ' , angle of friction defined in effective terms; c' , cohesion defined in effective terms; k_h and k_v , coefficients of permeability in horizontal and vertical directions. Table 3 indicates for the clay the variation with depth of the at-rest earth pressure coefficient, K_{op} , and undrained shear strength, c_u (σ'_{v0} , at-rest vertical effective stress), obtained from Equations 4 and 5. The clay is moderately over-consolidated to depth of 3 m and normally consolidated from 3 to 9 m. The values adopted for the clay

are similar to those used by Finno et al. (1991) regarding an excavation in soft soils constructed in Chicago, USA.

As to the smear zone, its cross-section is set as twice the area of the mandrel (Table 1), as considered by Lam et al. (2015). According to Bo et al. (2003), the ratio of horizontal permeability in the undisturbed zone and horizontal permeability in the smear zone (k_h/k_s) can vary from 1.5 to 5 depending on the type of drain, soil properties and installation procedures. In this study k_h/k_s is set as 2.

5. Analysis of results

One of the limitations usually existent in the design of embankments over soft ground is the low shear strength of the soft soils, which limits the load magnitude that can be applied with adequate safety for short term stability. In order to analyse stability for cases C1-C5, Figure 9 depicts overall safety factor (F) versus time, calculated from the 3D finite element results with the computer program for stability analysis described in Section 3.2. Figure 10 depicts the critical slip surfaces – and corresponding overall safety factors – at the end of construction and end of consolidation. Tables 4 and 5 illustrate the sums of acting and resisting forces along such critical surfaces. The parts of sums along the soft soil (foundation) and the fill (embankment) are also indicated.

These results show that, at the end of construction, the safety factor is very low for case C1 ($F = 1.09$), the case with

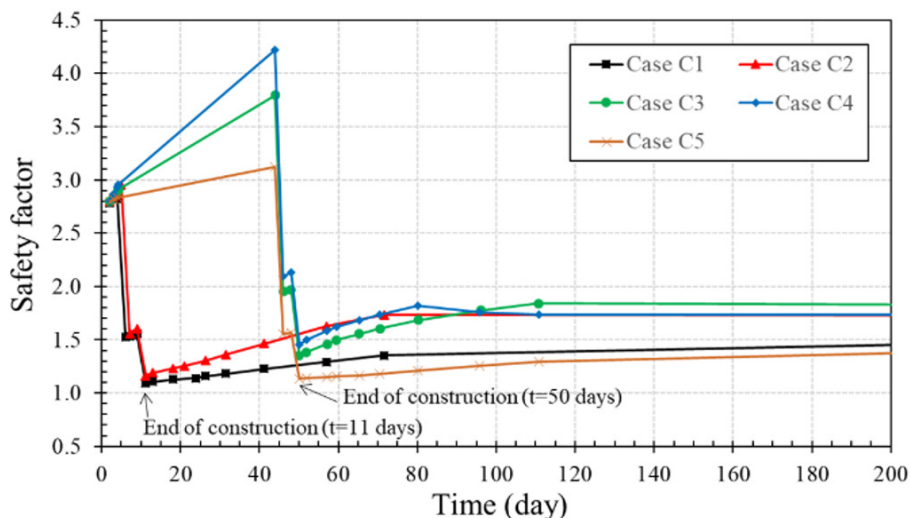


Figure 9. Overall safety factor versus time, for cases C1-C5.

Table 2. Geotechnical properties of the clay and embankment soil.

	γ (kN/m ³)	ν'	ϕ' (°)	c' (kPa)	k_h (m/s)	k_v (m/s)	p - q - θ critical state model			
							λ	k	Γ	N
Clay	16	0.25	26	0	10 ⁻⁹	10 ⁻⁹	0.18	0.025	3.05	3.158
Embankment	20	0.30	35	0	-	-	0.03	0.005	1.80	1.817

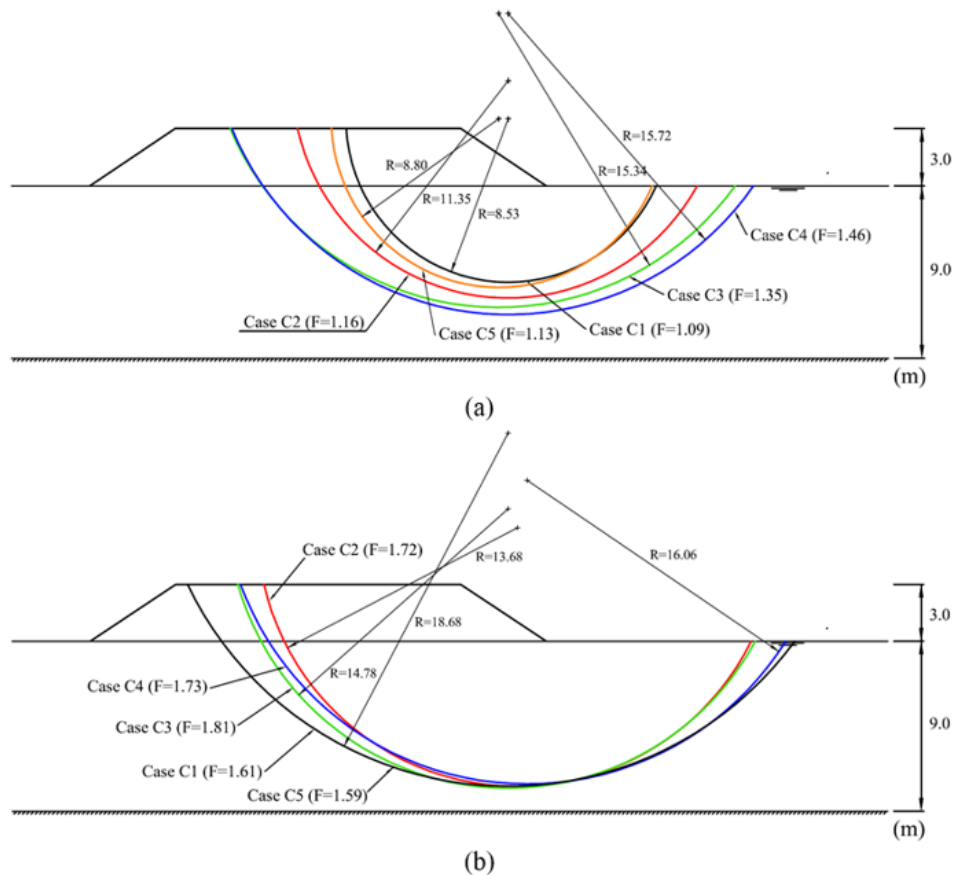


Figure 10. Critical slip surfaces for cases C1-C5: (a) end of construction; (b) end of consolidation.

Table 3. At rest earth pressure coefficient, K_0 , and undrained shear strength, c_u , of the clay.

Depth (m)	K_0	c_u (kPa)
0 - 3	0.9 - 0.5	13.0 - 4.9
≥ 3	0.5	$0.272\sigma'_{v0}$

a short time of construction (11 days) and without vacuum pressure. Although vacuum pressure is applied in case C2, its safety factor ($F = 1.16$) is only slightly higher than that of case C1. This shows that the effect of vacuum preloading on the safety is not efficient enough during construction unless a higher time of construction is considered. This is corroborated comparing cases C3-C5, whose construction time includes a pause period of 42 days after 1 m of embankment height (Figure 7b). For the case without vacuum pressure (case C5), the safety factor is also low ($F = 1.13$), while, for cases C3 and C4, F increases significantly, taking values of 1.35 and 1.46, respectively. This is explained by the higher gradients of excess pore pressure in cases C3 and C4, determined by the hydraulic boundary conditions on the PVDs, where excess pore pressure is set as -60 kPa and -90 kPa, respectively – while, for case C5, excess pore pressure is set as zero. The higher the gradients of excess pore pressure, the higher the

acceleration of the consolidation during the pause period and, therefore, the higher the values of F . As shown in Figure 9, in cases C3 and C4, F significantly increases during the pause period (until day 44) and diminishes during the subsequent phases of loading (embankment construction from 1 m to 2 m height – days 45 and 46 – and from 2 m to 3 m – days 49 and 50).

It should be noted that, at the beginning of the pause period of cases C3-C5, the maximum positive value of excess pore pressure is about 20 kPa (1 m of embankment height), which means that, for case C5 (without vacuum pressure, i.e. with minimum excess pore pressure equal zero), the gradients of excess pore pressure are relatively low and therefore the effect of consolidation during the pause period is lower than in cases C3 and C4 (Figure 9). This explains why the value of F at the end of construction in case C5 ($F = 1.13$) is only slightly higher than in case C1 ($F = 1.09$), despite its longer construction period.

The low values of F at the end of construction (3 m of embankment height) for the cases without vacuum application (slightly higher than 1, the value of overall failure) also show that the traditional technique of embankment surcharge (embankment fill with a higher height than 3 m, in this case) could not be applied in the current embankment, due to

Table 4. Critical slip surfaces at the end of construction for cases C1-C5: overall safety factor (F) and sums of acting and resisting forces.

	X_0 (m)	Y_0 (m)	R (m)	Sum of acting forces (kN)			Sum of resisting forces (kN)			F
				Total $\sum_{i=1}^N \tau_i A_i$	Foundation $\sum_{i=1}^{N1} \tau_i A_i$	Embankment $\sum_{i=1}^{N2} \tau_i A_i$	Total $\sum_{i=1}^N \tau_{fi} A_i$	Foundation $\sum_{i=1}^{N1} \tau_{fi} A_i$	Embankment $\sum_{i=1}^{N2} \tau_{fi} A_i$	
Case C1	10.0	12.5	8.53	138.67	126.91	11.76	151.06	135.20	15.86	1.09
Case C2	10.0	14.5	11.35	177.83	166.35	11.48	207.01	190.25	16.76	1.16
Case C3	9.5	18.0	15.34	230.52	220.22	10.30	311.20	294.37	16.83	1.35
Case C4	10.0	18.0	15.72	242.93	234.96	7.97	354.92	339.68	15.24	1.46
Case C5	9.5	12.5	8.80	145.39	136.04	9.35	164.36	149.17	15.19	1.13

R – radius; (X_0, Y_0) – co-ordinates of centre; $N=N_1+N_2$

Table 5. Critical slip surfaces at the end of consolidation for cases C1-C5: overall safety factor (F) and sums of acting and resisting forces.

	X_0 (m)	Y_0 (m)	R (m)	Sum of acting forces (kN)			Sum of resisting forces (kN)			F
				Total $\sum_{i=1}^N \tau_i A_i$	Foundation $\sum_{i=1}^{N1} \tau_i A_i$	Embankment $\sum_{i=1}^{N2} \tau_i A_i$	Total $\sum_{i=1}^N \tau_{fi} A_i$	Foundation $\sum_{i=1}^{N1} \tau_{fi} A_i$	Embankment $\sum_{i=1}^{N2} \tau_{fi} A_i$	
Case C1	10.0	20.0	18.68	291.62	293.38	-1.76	470.55	452.23	18.32	1.61
Case C2	10.5	15.0	13.68	259.47	256.25	3.22	446.59	425.03	21.56	1.72
Case C3	10.0	16.0	14.78	280.09	277.12	2.97	506.21	478.78	27.43	1.81
Case C4	11.0	17.5	16.06	291.66	289.88	1.78	505.18	480.43	24.75	1.73
Case C5	10.0	20.0	18.68	289.41	289.78	-0.37	460.64	441.21	19.43	1.59

R – radius; (X_0, Y_0) – co-ordinates of centre; $N=N_1+N_2$

overall instability. Surcharges of 60 and 90 kPa (equivalent to the vacuum preloads applied in cases C2-C4) correspond to additional fill heights of 3 and 4.5 m, respectively. These embankment heights, added to the 3 m high embankment, meant, therefore, that 6 m and 7.5 m high embankments needed to be constructed. As said, for these heights, with the same staged construction conditions, overall failure of the embankment would occur, contrary to what happens in the cases with vacuum application. As mentioned in section 1, this is one of the advantages of the vacuum technique when compared with the traditional technique of embankment surcharge.

After the end of construction, due to the consolidation process, the safety factor increases in all five cases (Figure 9), showing higher increase rates in the cases with vacuum preloading, which is due to the higher gradients of excess pore pressure at the end of construction due to the negative excess pore pressure on the PVDs, as explained above and shown below (Figures 11-15). At the end of consolidation, F takes higher values for the cases with vacuum application. This is explained by a certain improvement effect due to the preloading, determined by different stress paths during the construction and post-construction periods. Therefore, due to the elastoplastic behaviour of the soil, different effective stress redistributions occur which explains the differences in the results. This effect also reflects itself in lower deviatoric (distortion) strains within the soft soil at the end of consolidation

in the cases with vacuum application, which determines lower horizontal displacements under the embankment toe and lower settlements, as shown below.

After the end of vacuum application, the safety factor practically does not change for cases C2 and C3 and slightly diminishes for case C4, which means that, at the instant of the vacuum withdrawal, the consolidation is globally processed for the load of the 3 m-high embankment. This is corroborated below in the analysis of the settlements.

Figures 11-15 show the distributions of excess pore pressure at the end of construction and 1 month after the end of construction, for cases C1-C5. These figures depict results both on 3D axonometric perspectives where the vertical plane that contains one row of drain centres ($z = 0.75$ m plane) is visible (left side figures), and on 3D perspectives where the vertical plane equidistant from two rows of drains ($z = 0$ plane) is shown (right side figures). The scale of the colours is the same in all these figures, so that the results can be better compared. The shape of the isovalue lines clearly shows the three-dimensional condition of the problem, with drainage occurring both horizontally and vertically toward the several drainage surfaces (PVDs and upper drainage surface). At the end of construction, the highest value of excess pore pressure – which, as expected, takes place on the vertical plane equidistant from two rows of drains ($z = 0$) near the $x = 0$ symmetry plane –, occurs for case C1 (67.64 kPa) and is slightly higher than the maximum values of cases

C5 (64.63 kPa) and C2 (64.22 kPa) and significantly higher than those of cases C3 and C4 (49.29 kPa and 42.27 kPa, respectively). Therefore, similarly to the results of the stability,

these results show that, comparing with case C1 (without vacuum pressure), in case C2 the vacuum application does not significantly affect the maximum value of excess pore

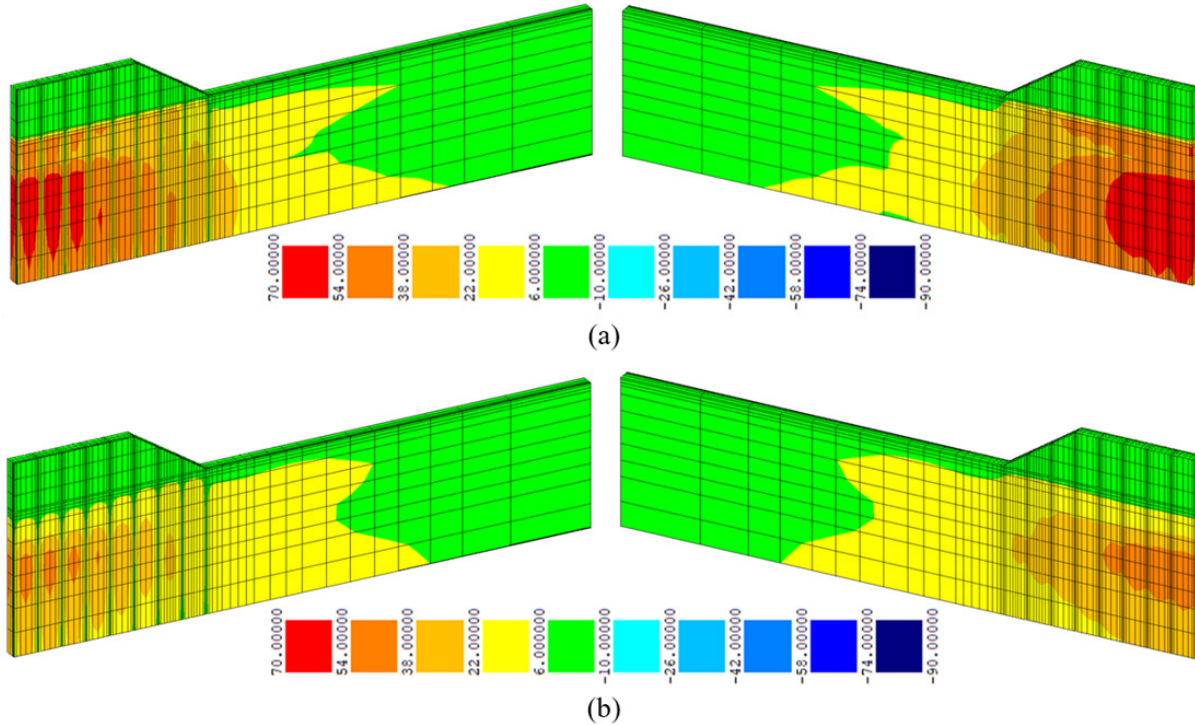


Figure 11. Excess pore pressure (u) for case C1 (without vacuum pressure; $u_{min} = 0$): (a) end of construction ($t = 11$ days) ($u_{max} = 67.64$ kPa); (b) 1 month after the end of construction ($u_{max} = 47.72$ kPa).

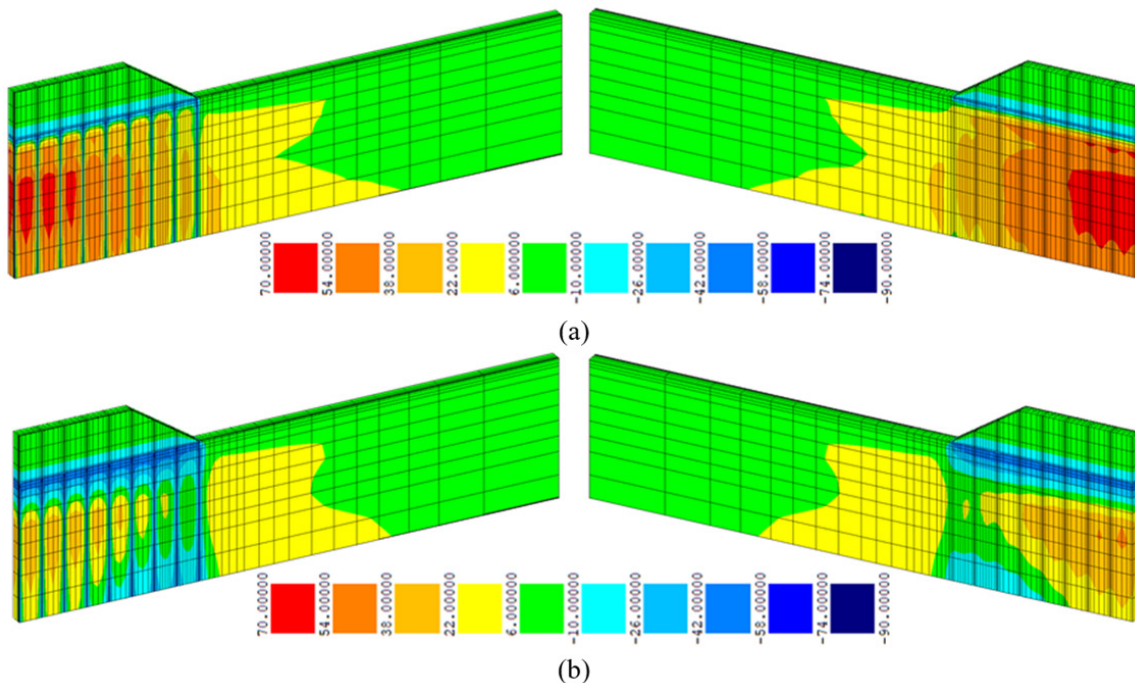


Figure 12. Excess pore pressure (u) for case C2 (vacuum pressure = -60 kPa; $u_{min} = -60$ kPa): (a) end of construction ($t = 11$ days) ($u_{max} = 64.22$ kPa); (b) 1 month after the end of construction ($u_{max} = 40.47$ kPa).

pressure during the construction period (due to its short time of construction), contrarily to what happens in cases C3 and C4 compared to case C5. After the construction period, when the problem is characterized by a transient flow of water, the isovalue lines (which geometrically coincide with

the equipotential lines) have a regular shape, normal to the flow lines of water.

It should be noted that, due to the elastoplastic behaviour of the soil, there are stress redistributions – both within the embankment material and within the soft soil – which are

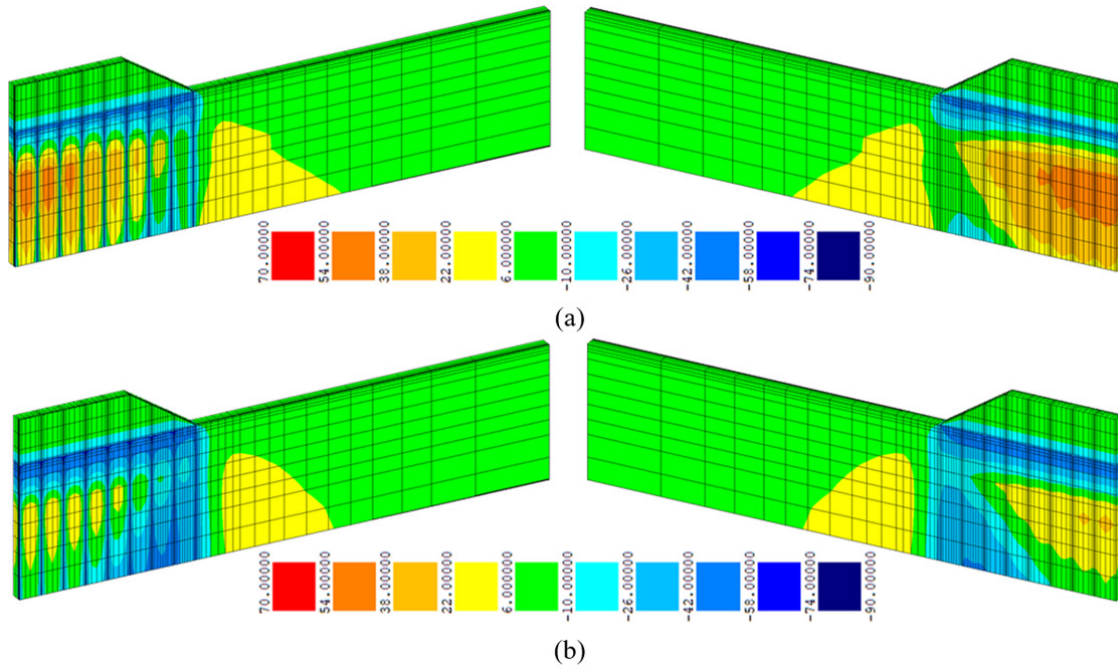


Figure 13. Excess pore pressure (u) for case C3 (vacuum pressure=-60 kPa; $u_{min} = -60$ kPa): (a) end of construction ($t = 50$ days) ($u_{max} = 49.29$ kPa); (b) 1 month after the end of construction ($u_{max} = 25.31$ kPa).

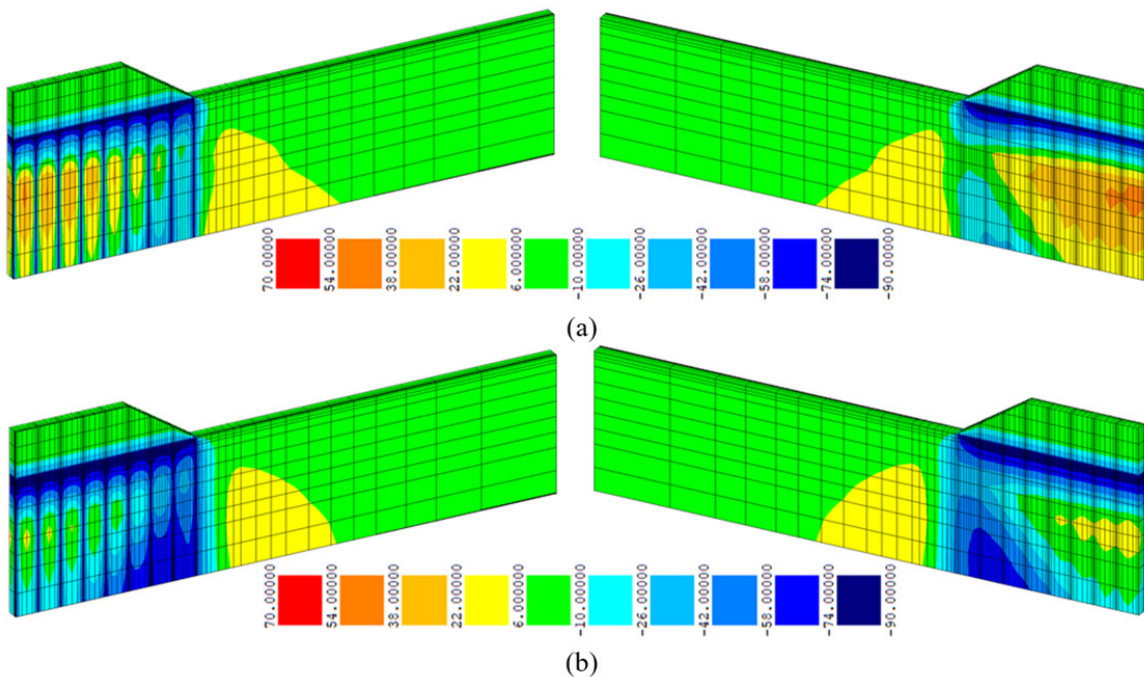


Figure 14. Excess pore pressure (u) for case C4 (vacuum pressure=-90 kPa; $u_{min} = -90$ kPa): (a) end of construction ($t = 50$ days; $u_{max} = 42.27$ kPa); (b) 1 month after the end of construction ($u_{max} = 17.25$ kPa).

globally related to the unconfined behaviour of the problem (occurrence of outward horizontal displacements in the lateral areas and non-uniform settlements at the embankment base) This implies that, globally, due to such stress redistributions, the total vertical stress transferred to the foundation soil tends to increase a little at the central zone under the embankment, while it tends to diminish in the lateral zones (Borges, 1995, 2004). This is why maximum values of excess pore pressure at the end of construction, for cases C1, C2 and C5, are a little higher than 60 kPa (value of 3 m height of embankment material) in the central zone of the foundation soil (Figures 11, 12 and 15).

The following figures depict for cases C1-C5: the evolution in time of settlement at the midpoint of the embankment base

(Figure 16); vertical displacements on the soft soil surface, at the end of construction and end of consolidation (Figure 17); horizontal displacements under the embankment toe, at the end of construction and end of consolidation (Figure 18).

The results of Figure 16 show that, after the end of vacuum application, the settlement at the midpoint of the embankment base practically does not change for case C2 and slightly diminishes for cases C3 and C4. This means that, in case C2, the instant of the vacuum withdrawal approximately corresponds to the time the consolidation is globally processed for the final load of the 3-m-high embankment. In cases C3 and C4, as said, after the end of the vacuum application, the ground surface has lifted a bit, which means that, in these cases, the time needed for the consolidation of the final load

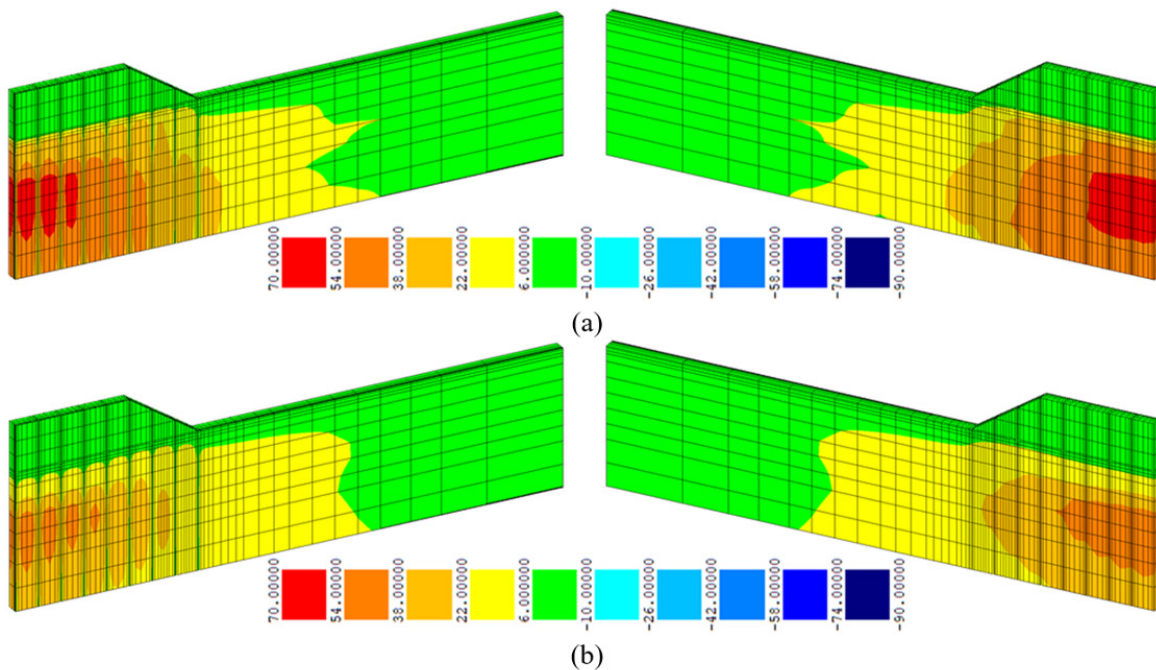


Figure 15. Excess pore pressure (u) for case C5 (without vacuum pressure; $u_{min} = 0$): (a) end of construction ($t = 50$ days; $u_{max} = 64.63$ kPa); (b) 1 month after the end of construction ($u_{max} = 48.94$ kPa).

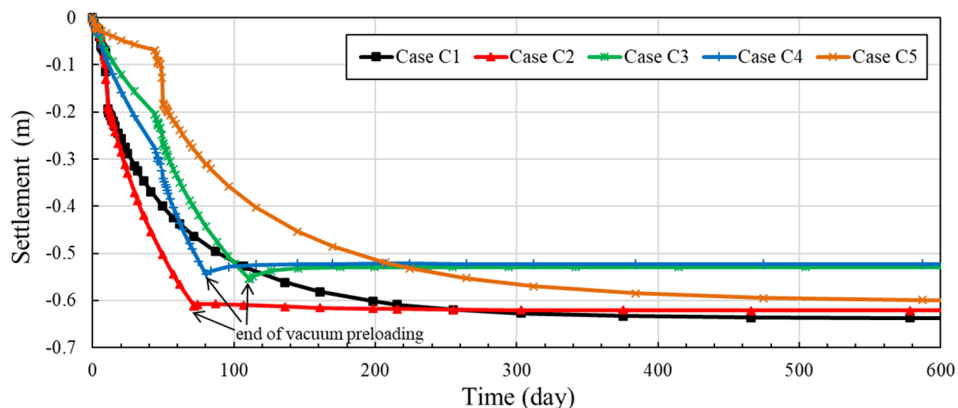


Figure 16. Settlement versus time at midpoint of the embankment base (co-ordinates: $x = 0$; $y = 9$ m; $z = 0$).

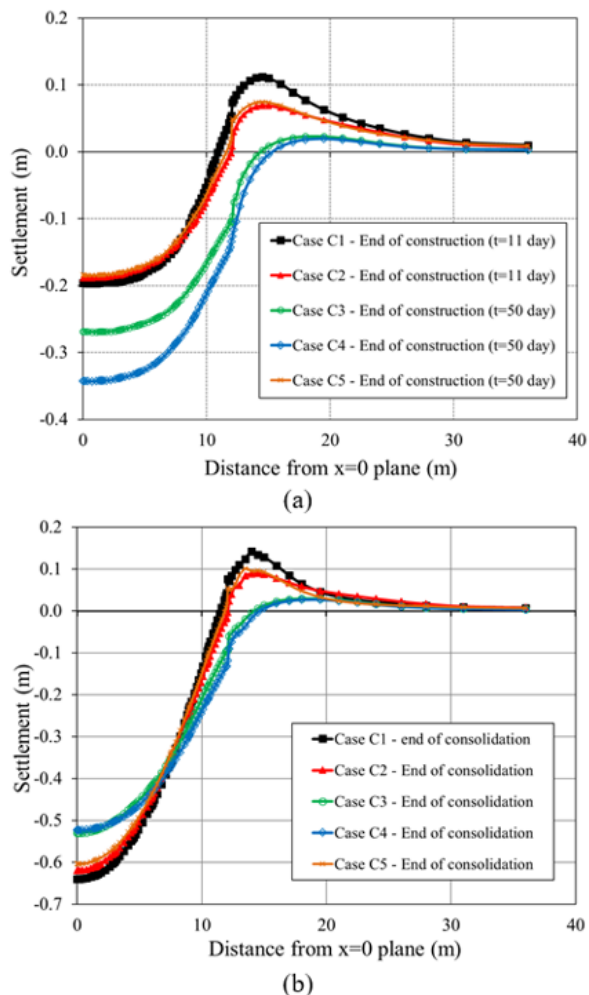


Figure 17. Vertical displacements on the soft soil surface ($y = 9$ m; $z = 0$): (a) end of construction; (b) end of consolidation.

of the 3 m-high embankment is a little shorter. Therefore, if the duration of vacuum application in cases C3 and C4 was a little shorter, negligible settlements could still be obtained after the end of vacuum application.

The results also show (Figures 16 and 17b) that the values of long-term settlement for cases C3 and C4 (52.9 cm and 52.2 cm, respectively) are significantly smaller than that of case C5 (60.4 cm). This reduction of long-term settlement (as well as reduction of horizontal displacements under the embankment toe, as shown below) is justified by a certain improvement effect of the soft soil – hardening effect (Borges, 2004; Borges & Almeida, 2018) – due to the vacuum application during the pause period for cases C3 and C4. Since the stress level of soft soil globally reduces during the pause period in cases C3 and C4, after that period, at the end of construction and for the post-construction period, stress levels are therefore also lower (as shown below). The lower the stress levels the lower the deviatoric (distortion)

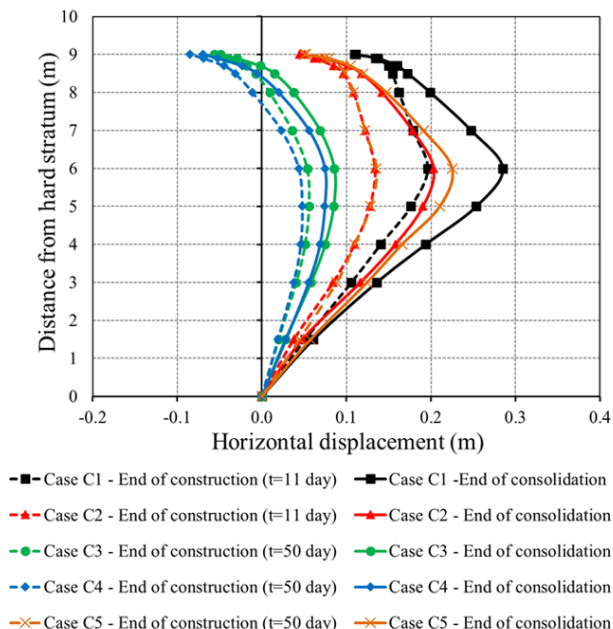


Figure 18. Horizontal displacements under the embankment toe ($x = 12$ m; $z = 0$).

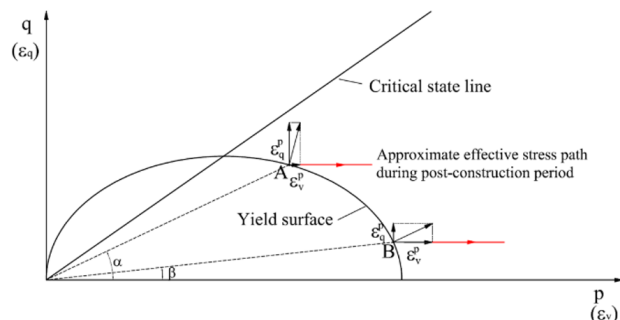


Figure 19. Yield and critical state surfaces of the p - q - θ critical state model in the p - q plane.

strains and, therefore, the smaller the settlements and the horizontal displacements at the end of consolidation.

In order to better illustrate this issue, Figure 19 shows, in p - q plane, the yield and critical state surfaces of the p - q - θ model (used to model the constitutive behaviour of soil); p is the effective mean stress and q the deviatoric stress. In the p - q plane, the yielding function is an ellipse. Two different stress states, points A and B, are depicted in Figure 19, with different values of stress level, SL (SL is higher at point A, since the angle α is higher than β). Since the plastic strain vector is normal to the yield surface, plastic deviatoric strain is higher at point A than at point B; i.e. the higher the stress level the higher the deviatoric strain. Therefore, once deviatoric strain (ϵ_q) implies outward horizontal displacement and settlement under the embankment, this is why settlements (as well as horizontal displacements under the embankment toe, as shown below) at the end of consolidation are larger for the cases without vacuum application (cases C1

and C5) and for case C2 (without a pause period after 1 m embankment construction), than for cases C3 and C4.

Regarding the vertical displacements on the soft soil surface (Figure 17), although maximum long-term settlements are lower for cases C3 and C4 (as commented above), their settlements at the end of construction are significantly larger than those of cases C1, C2 and C5. This is explained by their higher acceleration of consolidation during the construction period, due to higher gradients of excess pore pressure, as explained above, determining therefore significant consolidation settlements during that period. This is logically in consonance with the results of the safety factor, F , analysed above.

As to the upward displacements in the lateral regions of the embankment (Figure 17) and horizontal displacements under the toe (Figure 18), they are significantly smaller for cases C3 and C4 than for cases C1, C2 and C5. As said in section 1, one advantage of the vacuum application is its induction of

gradients of pore pressure in the ground maintaining a constant total stress. This therefore determines that the volume reduction provoked by the corresponding process of consolidation is associated with downward vertical displacements and inward horizontal displacements. This effect is contrary to what happens in the loading phases where upward vertical displacements in the lateral regions and outward horizontal displacements occur, which justifies the lower values for cases C3 and C4. On the other hand, as explained above regarding Figure 19, since stress levels are lower in cases C3 and C4, lower plastic deviatoric strains and higher plastic volumetric strains also occur, which increase the mentioned reduction effect of the outward horizontal displacements in the lateral regions of the embankment, as well as of the upward displacements.

Figure 20 shows colour maps of stress level for cases C1-C5 at the end of construction and end of consolidation (the figures depict results on 3D perspectives where the vertical

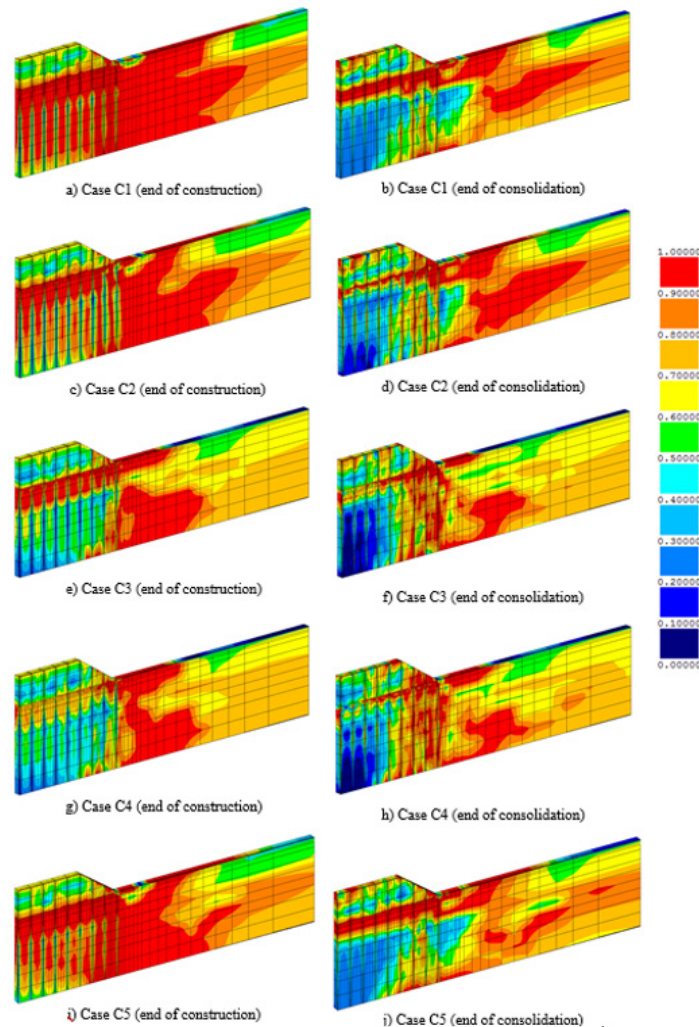


Figure 20. Stress level (SL) at the end of construction and end of consolidation, for cases C1-C5: (a) case C1 (end of construction); (b) case C1 (end of consolidation); (c) case C2 (end of construction); (d) case C2 (end of consolidation); (e) case C3 (end of construction); (f) case C3 (end of consolidation); (g) case C4 (end of construction); (h) case C4 (end of consolidation); (i) case C5 (end of construction); (j) Case C5 (end of consolidation).

plane that contains one row of drain centres is visible). Stress level, SL , measures the proximity to the soil critical state and is defined as follows:

$$SL = \frac{q}{pM} \quad (6)$$

where p is the effective mean stress, q the deviatoric stress and M the parameter that defines the slope of the critical state line in the p - q plane, as said above (Section 2). In normally consolidated soils, SL ranges from zero to 1, the latter being the critical state level. In over-consolidated soils, because of the peak strength behaviour, the stress level may be higher than 1.

The results of Figure 20 are logically in consonance with the results of stability analysed above. At the end of construction, the area with high values of stress level (due to the increase of deviatoric stress, q , during the loading phases) is much lower in cases C3 and C4 than in case C5 (and in cases C1 and C2). As said above, this difference is related with the consolidation effect due to the vacuum application during the construction period for cases C3 and C4, which increases the effective mean stress, p , and therefore reduces SL (see equation 6).

During the post-construction period, the effective stress path is globally characterized by an increase of the effective mean stress and a low variation of the deviatoric stress (Borges, 1995, 2004; Borges & Almeida, 2018). This implies that a generalised reduction of stress level occurs in all cases in response to the consolidation (Figure 20). However, this reduction is logically lower for cases C3 and C4, since, for these cases, part of the consolidation effect occurs during the construction period, as mentioned. Comparing all five cases, differences in the stress level maps are much less significant at the end of consolidation than at the end of construction, which, as expected, corroborates the results of safety factor, F , analysed above.

6. Conclusions

A computer code based on the finite element method was used to model 3D fully mechanical-hydraulic coupled analyses of an embankment on soft soils incorporating PVDs combined with vacuum preloading. A method for 3D overall stability study – which uses the numerical results obtained by the finite element code – was also proposed and applied. A parametric study was performed so that the influence of the magnitude of the vacuum preload and the staged construction of the embankment (time of vacuum application before completion of the embankment) was studied. The following conclusions can be highlighted:

- (1) At the end of construction, the safety factor was very low for the case without vacuum application and with a short time of construction (case C1). In

the case with vacuum application and the same time of construction (case C2), the safety factor was only slightly higher. This showed that the effect of vacuum preloading on the safety is not efficient enough during construction unless a higher time of construction is considered. This was corroborated comparing cases C3-C5, whose construction time included a pause period of 42 days after 1 m of embankment height. For the case without vacuum pressure (case C5), the safety factor, F , was also low, while, for cases C3 and C4, F significantly increased.

- (2) After the end of construction, the safety factor increased in all five cases, with higher increase rates for the cases with vacuum preloading (C2, C3 and C4). This is explained by the higher gradients of excess pore pressure at the end of construction in these cases, determined by the boundary conditions of excess pore pressure on the PVDs (-60 kPa for cases C2 and C3, and -90 kPa for case C4).
- (3) Long term settlements for cases C3 and C4 were significantly smaller than those of cases C1, C2 and C5. This is justified by a certain improvement effect of the soft soil, associated to lower stress levels, due to the vacuum application during the pause period.
- (4) When vacuum pressure is applied, the volume reduction provoked by the corresponding process of consolidation is associated with downward vertical displacements and inward horizontal displacements in the lateral regions of the embankment – contrarily to what happens in the loading phases. This justifies that upward displacements in the lateral regions and outward horizontal displacements under the embankment toe were significantly smaller for cases C3 and C4 than for the other cases.
- (5) At the end of construction, the area with high values of stress level was much lower in the cases with vacuum application and a longer time of construction (cases C3 and C4). This is justified by the consolidation acceleration during the pause period for these cases, determined by the hydraulic boundary conditions on the PVDs.
- (6) During the post-construction period, a generalised reduction of stress level occurred in all cases in response to the consolidation.

Acknowledgements

This work was financially supported by: Base Funding - UIDB/04708/2020 of the CONSTRUCT - Instituto de I&D em Estruturas e Construções - funded by national funds through the FCT/MCTES (PIDDAC).

Declaration of interest

The author has no conflicts of interest to declare.

List of symbols

c'	Cohesion defined in effective terms
c_u	Undrained shear strength
k_h	Coefficient of permeability in horizontal direction
k_v	Coefficient of permeability in vertical direction
p	Effective mean stress
p_i	Effective mean stress at i -polygon
p_v	Vacuum pressure
q	Deviatoric stress
q_w	Discharge capacity of the drain
t	Time
u	Excess pore pressure
u_{max}	Maximum excess pore pressure
A_i	Area of the i -polygon
F	Overall safety factor
K_0	At-rest earth pressure coefficient
M	Parameter that defines the slope of the critical state line in the p - q plane
N	Number of mesh elements intersected by the failure surface
N	Specific volume of normally consolidated soil at mean normal effective stress equal to 1 kPa
SL	Stress level
α_p	p -value of the centre of the yield surface in p - q plane
α_{pi}	α_p -value at i -polygon
γ	Soil unit weight
ε_q	Deviatoric strain
ε_v	Volumetric strain
θ	Angular stress invariant
k	Slope of swelling and recompression line
λ	Slope of normal consolidation line and critical state line
v_i	Specific volume of soil at i -polygon
ν^*	Poisson's ratio for drained loading
σ'_{v0}	At-rest vertical effective stress
σ'_x	Normal effective stress in the x -direction
σ'_y	Normal effective stress in the y -direction
σ'_z	Normal effective stress in the z -direction
τ_{fi}	Soil shear strength at i -polygon
τ_i	Projection of the acting shear stress at the i -polygon on the slip direction (i.e. normal to z -axis)
$\tau_{xy}, \tau_{yz}, \tau_{zx}$	Shear stresses in the x - y - z space
ϕ'	Angle of friction defined in effective terms
Γ	Specific volume of soil on the critical state line at mean normal effective stress equal to 1 kPa
FE	Finite element
PVD	Prefabricated vertical drain

References

- Alves, A.N. (2012). *Cylindrical diaphragm walls in deep excavations in soft soils* [Unpublished MSc thesis]. University of Porto (in Portuguese).
- Azevedo, M.S. (2010). *Cylindrical excavations in soft soils retained by slurry walls* [Unpublished MSc thesis]. University of Porto (in Portuguese).
- Barros, L. (2015). *Berlin-type retaining walls combined with jet-grout or cutter soil mixing walls: Analysis by the finite element method* [Unpublished MSc thesis]. University of Porto (in Portuguese).
- Bergado, D.T., Balasubramaniam, A.S., Jonathan Fannin, R., & Holtz, R.D. (2002). Prefabricated vertical drains (PVDs) in soft Bangkok clay: a case study of the new Bangkok International Airport project. *Canadian Geotechnical Journal*, 39(2), 304-315. <http://dx.doi.org/10.1139/t01-100>.
- Bo, M.W., Chu, J., Low, B.K., & Choa, V. (2003). *Soil improvement: prefabricated vertical drain techniques*. Singapore: Thomson Learning.
- Borges, J.L. (1995). *Geosynthetic-reinforced embankments on soft soils - Analysis and design* [Unpublished PhD Thesis]. Faculty of Engineering, University of Porto (in Portuguese).
- Borges, J.L. (2004). Three-dimensional analysis of embankments on soft soils incorporating vertical drains by finite element method. *Computers and Geotechnics*, 31(8), 665-676. <http://dx.doi.org/10.1016/j.compgeo.2004.11.001>.
- Borges, J.L., & Almeida, F. (2018). Sidewalls and PVDs below embankments on soft soils – three-dimensional analysis by FEM. *Geosynthetics International*, 25(6), 630-643. <http://dx.doi.org/10.1680/jgein.18.00030>.
- Borges, J.L., & Cardoso, A.S. (2001). Structural behaviour and parametric study of reinforced embankments on soft clays. *Computers and Geotechnics*, 28(3), 209-233. [http://dx.doi.org/10.1016/S0266-352X\(00\)00021-5](http://dx.doi.org/10.1016/S0266-352X(00)00021-5).
- Borges, J.L., & Cardoso, A.S. (2002). Overall stability of geosynthetic-reinforced embankments on soft soils. *Geotextiles and Geomembranes*, 20(6), 395-421. [http://dx.doi.org/10.1016/S0266-1144\(02\)00014-6](http://dx.doi.org/10.1016/S0266-1144(02)00014-6).
- Borges, J.L., & Gonçalves, M.S. (2016). Jet-grout column-reinforced soft soils incorporating multilayer geosynthetic-reinforced platforms. *Soil and Foundation*, 56(1), 57-72. <http://dx.doi.org/10.1016/j.sandf.2016.01.005>.
- Borges, J.L., & Guerra, G.T. (2014). Cylindrical excavations in clayey soils retained by jet grout walls: numerical analysis and parametric study considering the influence of consolidation. *Computers and Geotechnics*, 55, 42-56. <http://dx.doi.org/10.1016/j.compgeo.2013.07.008>.
- Borges, J.L., & Marques, D.O. (2011). Geosynthetic-reinforced and jet grout column-supported embankments on soft soils: numerical analysis and parametric study. *Computers and Geotechnics*, 38(7), 883-896. <http://dx.doi.org/10.1016/j.compgeo.2011.06.003>.
- Borges, J.L., & Santos, R.M. (2020). Bottom reinforcement in braced excavations: coupled analysis and new method for basal-heave stability study. *Soils and Rocks*, 43(2), 199-217. <http://dx.doi.org/10.28927/SR.432199>.
- Borges, J.L., Domingues, T.S., & Cardoso, A.S. (2009). Embankments on soft soil reinforced with stone columns:

- numerical analysis and proposal of a new design method. *Geotechnical and Geological Engineering*, 27(6), 667-679. <http://dx.doi.org/10.1007/s10706-009-9266-z>.
- Britto, A.M., & Gunn, M.J. (1987). *Critical soil mechanics via finite elements*. Ellis Horwood Limited, England.
- Caramelo, T.A. (2011). *Embankments on soft soils reinforced with jet grout columns and geosynthetics* [Unpublished MSc thesis]. Faculty of Engineering, University of Porto (in Portuguese).
- Cascone, E., & Biondi, G. (2013). A case study on soil settlements induced by preloading and vertical drains. *Geotextiles and Geomembranes*, 38, 51-67. <http://dx.doi.org/10.1016/j.geotexmem.2013.05.002>.
- Chai, J., & Rondonuwu, S.G. (2015). Surcharge loading rate for minimizing lateral displacement of PVD improved deposit with vacuum pressure. *Geotextiles and Geomembranes*, 43(6), 558-566. <http://dx.doi.org/10.1016/j.geotexmem.2015.07.012>.
- Chai, J., Miura, N., Sakajo, S., & Bergado, D. (1995). Behavior of vertical drain improved subsoil under embankment loading. *Soil and Foundation*, 35(4), 49-61. http://dx.doi.org/10.3208/sandf.35.4_49.
- Chai, J.C., Carter, J.P., & Hayashi, S. (2005). Ground deformation induced by vacuum consolidation. *Journal of Geotechnical and Geoenvironmental Engineering*, 131(12), 1552-1561. [http://dx.doi.org/10.1061/\(ASCE\)1090-0241\(2005\)131:12\(1552\)](http://dx.doi.org/10.1061/(ASCE)1090-0241(2005)131:12(1552)).
- Chen, J.F., Li, L.Y., Xue, J.F., & Feng, S.Z. (2015). Failure mechanism of geosynthetic-encased stone columns in soft soils under embankment. *Geotextiles and Geomembranes*, 43(5), 424-431. <http://dx.doi.org/10.1016/j.geotexmem.2015.04.016>.
- Costa, P.A. (2005). *Braced excavations in soft clayey soils: Behavior analysis including the consolidation effects* [Unpublished MSc Thesis]. Faculty of Engineering, University of Porto (in Portuguese).
- Costa, P.A., Borges, J.L., & Fernandes, M.M. (2007). Analysis of a braced excavation in soft soils considering the consolidation effect. *Geotechnical and Geological Engineering*, 25(6), 617-629. <http://dx.doi.org/10.1007/s10706-007-9134-7>.
- Domingues, T.S. (2006). *Foundation reinforcement with stone columns in embankments on soft soils: Analysis and design* [Unpublished MSc Thesis]. Faculty of Engineering, University of Porto (in Portuguese).
- Finno, R.J., Harahap, I.S., & Sabatini, P.J. (1991). Analysis of braced excavations with coupled finite element formulations. *Computers and Geotechnics*, 12(2), 91-114. [http://dx.doi.org/10.1016/0266-352X\(91\)90001-V](http://dx.doi.org/10.1016/0266-352X(91)90001-V).
- Gonçalves, M.A. (2012). *Embankments on soft soils reinforced with jet-grout columns and multilayer geosynthetic-reinforced load transfer platforms* [Unpublished MSc Thesis]. Faculty of Engineering, University of Porto (in Portuguese).
- Guerra, G.T. (2009). *Self-supported jet-grout walls in cylindrical excavations* [Unpublished MSc Thesis]. University of Porto (in Portuguese).
- Hinchberger, S.D., & Rowe, R.K. (2003). Geosynthetic reinforced embankments on soft clay foundations: predicting reinforcement strains at failure. *Geotextiles and Geomembranes*, 21(3), 151-175. [http://dx.doi.org/10.1016/S0266-1144\(03\)00006-2](http://dx.doi.org/10.1016/S0266-1144(03)00006-2).
- Hird, C.C., Pyrah, I.C., & Russell, D. (1992). Finite element modelling of vertical drains beneath embankments on soft ground. *Geotechnique*, 42(3), 499-511. <http://dx.doi.org/10.1680/geot.1992.42.3.499>.
- Holtz, R.D., Jamiolkowski, M., Lancellotta, R., & Pedroni, S. (1991). *Prefabricated Vertical Drains: Design and Performance*. London: Heinemann-CIRIA.
- Indraratna, B., & Redana, I.W. (2000). Numerical modeling of vertical drains with smear and well resistance installed in soft clay. *Canadian Geotechnical Journal*, 37(1), 133-145. <http://dx.doi.org/10.1139/t99-115>.
- Indraratna, B., Kan, M.E., Potts, D., Rujikiatkamjorn, C.W., & Sloan, S.W. (2016). Analytical solution and numerical simulation of vacuum consolidation by vertical drains beneath circular embankments. *Computers and Geotechnics*, 80, 83-96. <http://dx.doi.org/10.1016/j.compgeo.2016.06.008>.
- Indraratna, B., Rujikiatkamjorn, C., Balasubramaniam, A.S., & McIntosh, G. (2012). Soft ground improvement via vertical drains and vacuum assisted preloading. *Geotextiles and Geomembranes*, 30, 16-23. <http://dx.doi.org/10.1016/j.geotexmem.2011.01.004>.
- Lam, L.G., Bergado, D.T., & Hino, T. (2015). PVD improvement of soft Bangkok clay with and without vacuum preloading using analytical and numerical analyses. *Geotextiles and Geomembranes*, 43, 547-557. <http://dx.doi.org/10.1016/j.geotexmem.2015.07.013>.
- Lewis, R.W., & Schrefler, B.A. (1987). *The finite element method in the deformation and consolidation of porous media*. New York: John Wiley and Sons, Inc.
- Lin, D.G., & Chang, K.T. (2009). Three-dimensional numerical modelling of soft ground improved by prefabricated vertical drains. *Geosynthetics International*, 16(5), 339-353. <http://dx.doi.org/10.1680/gein.2009.16.5.339>.
- Liu, K.-W., & Rowe, R.K. (2015). Numerical modelling of prefabricated vertical drains and surcharge on reinforced floating column-supported embankment behaviour. *Geotextiles and Geomembranes*, 43(6), 493-505. <http://dx.doi.org/10.1016/j.geotexmem.2015.05.006>.
- Long, P.V., Nguyen, L.V., Bergado, D.T., & Balasubramaniam, A.S. (2015). Performance of PVD improved soft ground using vacuum consolidation methods with and without airtight membrane. *Geotextiles and Geomembranes*, 43, 473-483. <http://dx.doi.org/10.1016/j.geotexmem.2015.05.007>.
- Marques, D.O. (2008). *Reinforcement of foundation soils with jet-grout columns and geosynthetics* [Unpublished

- MSc Thesis]. Faculty of Engineering, University of Porto (in Portuguese).
- Marques, D.O. (2021). *Embankments on soft soils reinforced with stone columns: numerical and experimental analysis* [Unpublished PhD Thesis]. Faculty of Engineering, University of Porto (in Portuguese).
- Mesri, G., & Khan, A.Q. (2012). Ground Improvement using vacuum loading together with vertical drains. *Journal of Geotechnical and Geoenvironmental Engineering*, 138(6), 680-689. [http://dx.doi.org/10.1061/\(ASCE\)GT.1943-5606.0000640](http://dx.doi.org/10.1061/(ASCE)GT.1943-5606.0000640).
- Monteiro, A.S. (2011). *Excavations in clayey soils retained by jet-grout walls reinforced with steel beams* [Unpublished MSc Thesis]. University of Porto (in Portuguese).
- Pinto, M.S. (2011). *Excavations supported by reinforced concrete walls and slab bands* [Unpublished MSc Thesis]. University of Porto (in Portuguese).
- Rowe, R.K., & Soderman, K.L. (1987). Stabilization of very soft soils using high strength geosynthetics: the role of finite element analyses. *Geotextiles and Geomembranes*, 6, 53-80. [http://dx.doi.org/10.1016/0266-1144\(87\)90057-4](http://dx.doi.org/10.1016/0266-1144(87)90057-4).
- Rujikiatkamjorn, C., Indraratna, B., & Chu, J. (2008). 2D and 3D numerical modeling of combined surcharge and vacuum preloading with vertical drains. *International Journal of Geomechanics*, 8(2), 144-156. [http://dx.doi.org/10.1061/\(ASCE\)1532-3641\(2008\)8:2\(144\)](http://dx.doi.org/10.1061/(ASCE)1532-3641(2008)8:2(144)).
- Santos, R.M. (2014). *Basal-heave stability of strutted excavations in soft soils: Safety analysis by the finite element method* [Unpublished MSc Thesis]. University of Porto (in Portuguese).
- Saowapakpiboon, J., Bergado, D.T., Youwai, S., Chai, J.C., Wanthong, P., & Voottipruex, P. (2010). Measured and predicted performance of prefabricated vertical drains (PVDs) with and without vacuum preloading. *Geotextiles and Geomembranes*, 28(1), 1-11. <http://dx.doi.org/10.1016/j.geotexmem.2009.08.002>.
- Shen, S.L., Chai, J.C., Hong, Z.S., & Cai, F.X. (2005). Analysis of field performance of embankments on soft clay deposit with and without PVD improvement. *Geotextiles and Geomembranes*, 23(6), 463-485. <http://dx.doi.org/10.1016/j.geotexmem.2005.05.002>.
- Silva, E.M., Justo, J.L., Durand, P., Justo, E., & Vazquez-Boza, M. (2017). The effect of geotextile reinforcement and prefabricated vertical drains on the stability and settlement of embankments. *Geotextiles and Geomembranes*, 45(5), 447-461. <http://dx.doi.org/10.1016/j.geotexmem.2017.07.001>.
- Zhang, Z., Ye, G., & Xing, H. (2015). Consolidation analysis of soft soil improved with short deep mixed columns and long prefabricated vertical drains (PVDs). *Geosynthetics International*, 22(5), 366-379. <http://dx.doi.org/10.1680/jgein.15.00018>.
- Zhang, Z., Ye, G., & Xu, Y. (2018). Comparative analysis on performance of vertical drain improved clay deposit under vacuum or surcharge loading. *Geotextiles and Geomembranes*, 46(2), 146-154. <http://dx.doi.org/10.1016/j.geotexmem.2017.11.002>.